

# Compact spatio-spectral algorithm for single image super-resolution in hyperspectral imaging

## Superresolución basado en una única imagen para imágenes hiperespectrales

Miguel A. Marquez<sup>1</sup>, Cesar A. Vargas<sup>2</sup>, and H. Arguello<sup>3</sup>

### ABSTRACT

Hyperspectral imaging (HSI) is used in a wide range of applications such as remote sensing, space imagery, mineral detection, and exploration. Unfortunately, it is difficult to acquire hyperspectral images with high spatial and spectral resolution due to instrument limitations. The super-resolution techniques are used to reconstruct low-resolution hyperspectral images. However, traditional super-resolution (SR) approaches do not allow direct use of both spatial and spectral information, which is a decisive for an optimal reconstruction. This paper proposes a single image SR algorithm for HSI. The algorithm uses the fact that the spatial and spectral information can be integrated to make an accurate estimate of the high-resolution HSI. To achieve this, two types of spatio-spectral downsampling, and a three-dimensional interpolation are proposed in order to increase coherence between the spatial and spectral information. The resulting reconstructions using the proposed method are up to 2 dB better than traditional SR approaches.

**Keywords:** Hyperspectral imaging, spatio-spectral dimension, three-dimensional interpolation, hyperspectral downsampling.

### RESUMEN

Las imágenes hiperespectrales (HSI) son de vital importancia en una amplia gama de aplicaciones, tales como la teledetección, imágenes espaciales, la detección y la exploración de minerales. Desafortunadamente, es difícil adquirir HSI de alta resolución espacio-espectral debido a las limitaciones de los equipos de sensado. Para obtener versiones de HSI de alta calidad se usan técnicas tradicionales de superresolución. Estas técnicas no permiten el uso directo de la información espacial y espectral que son un factor decisivo para una óptima reconstrucción. En este trabajo se propone la implementación de un novedoso algoritmo de superresolución de una sola imagen hiperespectral. El algoritmo integra la información espacial y espectral en las HSI para realizar una estimación precisa de alta resolución. Esta integración se obtiene mediante el uso de dos tipos de muestreo espacio-espectral y un interpolador tridimensional, que permite aumentar la coherencia de la información inherente en la imagen. Las imágenes resultantes son superiores hasta 2 dB comparas con reconstrucciones obtenidas por enfoques tradicionales.

**Palabras clave:** Imágenes hiperespectrales, dimensión especial-espectral, interpolación tridimensional, sub-muestreo hiperespectral.

**Received:** October 2nd 2016

**Accepted:** November 8th 2016

### Introduction

Hyperspectral imaging (HSI) collects a concatenation of bidimensional images that entails different wavelengths in a certain spectral range. Pixels in hyperspectral images are therefore represented by vectors whose entries correspond to the intensity in the different spectral bands. HSI enables the detection, classification, and identification of objects and features based on the spectral characteristics (Chakrabarti, 2011). HSI is an area with a significant impact in civilian and military applications including remote sensing, aerial, space imagery, natural resource exploration, farming, and astronomy (Belluco, 2006), (Borengasser, 2007), (Castrodad, 2010), (Melgani, 2004), (Underwood, 2003), (Dicker, 2006), (Turk, 1991). In all of these applications, it is important to obtain the highest resolution in the spatial and spectral dimensions. Typically, the hyperspectral spectrometers are used to capture high-resolution hyperspectral images, because these provide hundreds of narrow contiguous bands over a

<sup>1</sup> BSc. in Computer Sciences and Masters Student in applied mathematics at Universidad Industrial de Santander, Colombia. Affiliation: Master at student Universidad Industrial de Santander, Colombia.

E-mail: hds.marquez@gmail.com.

<sup>2</sup> BSc. in Computer Sciences and MSc. in Computer Sciences at Universidad Industrial de Santander, Colombia. Ph.D student at University of Delaware, USA. Affiliation: Ph.D student at University of Delaware, USA.

E-mail: caugusto.vargas@gmail.com

<sup>3</sup> BSc in Electrical Engineering and MSc in Electrical Power at Universidad Industrial de Santander, Colombia. Ph.D in Electrical and Computer Engineering from the University of Delaware, USA. Affiliation: Associated professor at Universidad Industrial de Santander, Colombia.

E-mail: henarfu@uis.edu.co

**How to cite:** Marquez, M, A., Vargas, C, A., & Arguello, H. (2016). Compact spatio-spectral algorithm for single image super-resolution in hyperspectral imaging. *Ingeniería e Investigación*, 36(3), 117–124. DOI: 10.15446/ing.investig.v36n3.54267



Attribution 4.0 International (CC BY 4.0) Share - Adapt

wide range of the electromagnetic spectrum. Hyperspectral sensors measure the reflective properties of objects in the visible and short wave infrared regions of the spectrum. Unfortunately, atmospheric scattering, imperfect imaging optics, secondary illumination, changing viewing angles, and sensor noise degrade the quality of these images, making the spatial resolution one of the most expensive and hardest characteristic to be improved in imaging systems.

In practice, modifying the imaging optics or sensor array increases the production costs (Arguello H., 2012)- (Rueda, 2013); in addition it is impossible to fabricate spectrometers with arbitrary resolution. Hence, researchers have investigated the use of resolution enhancement techniques by post processing as a better alternative to improve the image quality (Akgun, 2005), (Mianji, 2008), (Zhao, 2011). To improve the spatial resolution of hyperspectral images, traditional super-resolution (SR) techniques may be used. Super-resolution methods are currently a very active area of research, as it allows the implementation of low-cost imaging sensors in hyperspectral spectrometers. Many methodologies have been applied to the super-resolution problem, such as SR from single image methods (Zhang, 2012), (Takeda, 2007), (Li, 2001), multi-image-based SR methods (Protter, 2009), (Akgun, 2005), (Chan, 2010), and learning-based SR methods (Freeman, 2002). However, these methods ignore the spectral information that is a crucial parameter for an optimal reconstruction of high resolution (HR) images. A comprehensive background on super-resolution methods can be found in (Akgun, 2005).

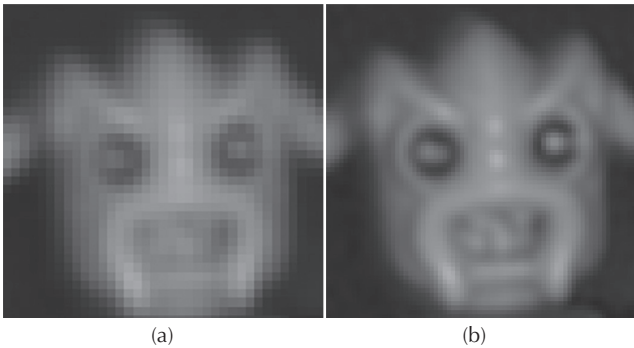


**Figure 1.** Restoration of a LR image by SR methods. (a) Depicts the input LR image  $\mathbf{Y} \in \mathbb{R}^{M \times N}$  with a super-resolution factor of  $s_1$ , and  $s_2$ . (b) Depicts the output HR image  $\mathbf{X} \in \mathbb{R}^{N_1 \times M_1}$ .

This paper focuses on the problem of recovering the super-resolution version of a given low-resolution hyperspectral image. Specifically, this work develops a novel reconstruction approach by which the spatio-spectral information of low-resolution (LR) HSI input is exploited. We named this novel super-resolution algorithm the C2SR algorithm. We suggest a fast algorithm to integrate the spatial and spectral information of an HSI to exploit the spatial resolution of the image. Moreover, C2SR can work on HSIs captured using current hyperspectral spectrometers. This becomes an advantage over other techniques like (Rueda-Chacón, 2014), (Arguello H. &, 2012), which require the re-design of spectrometers based on compressive sensing approaches.

## Methodology

### *Bidimensional image super-resolution*

The single image super-resolution (SR) problem consists on recovering a high resolution (HR) image  $\mathbf{X} \in \mathbb{R}^{s_1 N \times s_2 M}$  from a low resolution (LR)  $\mathbf{Y} \in \mathbb{R}^{N \times M}$  version. Figure 1 shows an example of an HR image restoration from an LR version of it. Here,  $N \times M$  represents the spatial resolution, and  $s_1, s_2 \in \mathbb{R}$  are the super-resolution factors in the dimensions  $N$  and  $M$ , respectively. Let  $\mathbf{X} \in \mathbb{R}^{s_1 s_2 N M \times 1}$  and  $\mathbf{y} \in \mathbb{R}^{N M \times 1}$  be the vector representations of a HR and its LR image version, respectively (Zhao, 2011), (Winter, 2002), (Tanaka, 2007). Then the sensed image can be expressed as

$$\mathbf{y} = \mathbf{D}\mathbf{H}\mathbf{x} + \boldsymbol{\varepsilon} \quad (1)$$

where  $\mathbf{H} \in \mathbb{R}^{s_1 s_2 N M \times s_1 s_2 N M}$  denotes the blurring matrix,  $\mathbf{D} \in \mathbb{R}^{N M \times s_1 s_2 N M}$  is the downsampling matrix, and  $\boldsymbol{\varepsilon} \in \mathbb{R}^{N M \times 1}$  is the noise introduced by the sensing system. Examples of the structure of the matrices  $\mathbf{D}$  and  $\mathbf{H}$  are indicated in Figure 2. Since,  $N M \ll s_1 s_2 N M$ , Equation (1) leads to an undetermined system of linear equations, which has infinite number of solutions on  $\mathbf{x}$ , i.e. an ill-posed problem. To make the image recovery process less ill-posed (Akgun, 2005), (Dong, 2011), Equation (1), can be rewritten as the least squares formulation

$$\hat{\mathbf{x}} = \underset{\mathbf{x}}{\operatorname{argmin}} \|\mathbf{y} - \mathbf{D}\mathbf{H}\mathbf{x}\|_2^2 \quad (2)$$

Solution to Equation (2) is given by

$$\hat{\mathbf{x}} = \mathbf{H}^T \mathbf{D}^T (\mathbf{D}\mathbf{H}\mathbf{H}^T \mathbf{D}^T)^{-1} \mathbf{y} \quad (3)$$

however, this method leads to a low quality spatial reconstruction image. To increase quality, several SR methods incorporate an effective prior (denoted as a regularization term) into the reconstruction process in order to improve the above solution. Accordingly, Equation (2) is reformulated as

$$\hat{\mathbf{x}} = \underset{\mathbf{x}}{\operatorname{argmin}} \|\mathbf{y} - \mathbf{D}\mathbf{H}\mathbf{x}\|_2^2 + \mu F(\mathbf{x}) \quad (4)$$



(a)

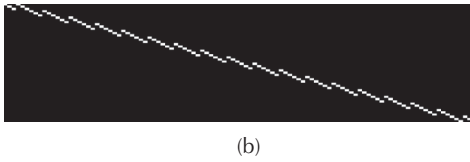


**Figure 2.** Example of a downsampling matrix  $\mathbf{D}_H \in \mathbb{R}^{54 \times 216}$ , and a blurring matrix  $\mathbf{H}_H \in \mathbb{R}^{216 \times 216}$  for a hyperspectral image  $\mathbf{X} \in \mathbb{R}^{35 \times 35 \times 6 \times s_3}$ , with a super-resolution factors of  $s_1 = s_2 = 2$ , and  $s_3 = 1$ . (a) Downsampling matrix  $\mathbf{D}_H$ . (b) The sensing matrix  $\mathbf{H}_H$  whose effect is equivalent to a symmetric Gaussian lowpass filter of size 3 with standard deviation  $\sigma = 1$ . The dark and white pixels depicts values 0 and 1, respectively.

where  $F(\mathbf{x})$  is a regularization prior, and  $\mu$  is a regularization parameter which represents the tradeoff between the reconstruction error and the regularization term. To evaluate the reconstruction performance of our method, we choose two traditional methods of SR. Non-local means (NLM), and steering kernel regression (SKR) are two important methods of super-resolution. These methods have received a substantial attention, being a family of methods based upon local smoothness assumption, i.e., the local structure is relatively stable (Takeda, 2007), (Protter, 2009).

### Hyperspectral image super-Resolution

Hyperspectral imaging entails signals typically spanning hundreds of contiguous wavelength bands in a certain spectral range. Pixels in hyperspectral images are therefore represented as vectors whose entries correspond to the intensity in different spectral bands. Let  $\mathbf{X}_H \in \mathbb{R}^{s_1 \times s_2 \times M \times s_3 \times L}$  be a high-resolution hyperspectral image (HR-HSI), and  $\mathbf{Y}_H \in \mathbb{R}^{N \times M \times L}$  its low-resolution (LR-HSI) version. Here,  $\mathbf{L}$  represents the spectral resolution, and  $s_3 \in \mathbb{R}$  is the super-resolution factor in the dimension  $\mathbf{L}$ . Also let  $\mathbf{x}_H \in \mathbb{R}^{s_1 s_2 s_3 N M L \times 1}$  and  $\mathbf{y}_H \in \mathbb{R}^{N M L \times 1}$  be the HR-HSI and LR-HSI vector representation of  $\mathbf{X}_H$  and  $\mathbf{Y}_H$  respectively. The HSI acquisition process of  $\mathbf{y}_H$  from  $\mathbf{x}_H$  can be modeled as

$$\mathbf{y}_H = \mathbf{D}_H \mathbf{H}_H \mathbf{x}_H + \boldsymbol{\epsilon}_H \quad (5)$$

where  $\mathbf{D}_H \in \mathbb{R}^{N M L \times s_1 s_2 s_3 N M L}$  is the downsampling matrix in the spatial and spectral domain,  $\mathbf{H}_H \in \mathbb{R}^{s_1 s_2 s_3 N M L \times s_1 s_2 s_3 N M L}$  is a matrix that describes the blurring in each spectral band (no blurring across the spectrum), and  $\boldsymbol{\epsilon}_H \in \mathbb{R}^{N M L \times 1}$  is the noise introduced by the sensing system. Examples of the matrices  $\mathbf{D}_H$  and  $\mathbf{H}_H$  are indicated in Figure 2. The signal  $\mathbf{x}_H$  can be estimated by solving

$$\hat{\mathbf{x}}_H = \underset{\mathbf{x}_H}{\operatorname{argmin}} \left\| \mathbf{y}_H - \mathbf{D}_H \mathbf{H}_H \mathbf{x}_H \right\|_2^2 \quad (6)$$

or approximated by using a gradient descent method such as

$$\mathbf{x}_H^{t+1} = \mathbf{x}_H^t + \tau (\mathbf{D}_H \mathbf{H}_H)^T (\mathbf{y}_H - \mathbf{D}_H \mathbf{H}_H \mathbf{x}_H) \quad (7)$$

Equation (5) is extremely ill-posed, considering that the product  $(\mathbf{D}_H \mathbf{H}_H)^T \mathbf{y}_H$  generates HR-HSI. The missing spectral bands are therefore set up with zeros; this effect is commonly known as zero-padding (Figure 3). Thus, the recover signal  $\mathbf{x}_H^{t+1}$  is a hyperspectral image with zero-padding in its spectral field, and this is inconsistent with the requirements of high-resolution HSI. Figure 3 depicts an image with zero-padding in its spectral fields.

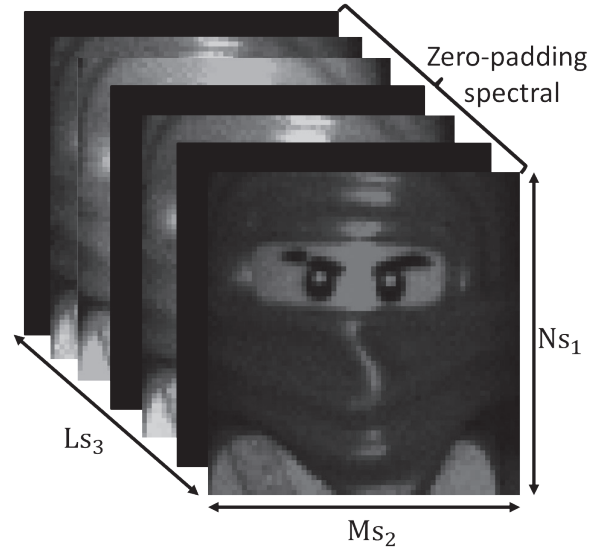


**Figure 3.** Reconstruction of a LR hyperspectral image ( $\mathbf{Y} \in \mathbb{R}^{3 \times 3 \times 3}$ ) by traditional methods using Equation (7).

### The compact spatio-spectral super-resolution algorithm (C2SR)

This work revisits the HSI super-resolution problem, proposing the compact spatio-spectral super-resolution approach. This approach solves two main problems in current HSI super-resolution techniques: zero-padding, and waste of spectral information. In summary, three major steps can describe the proposed algorithm. First, an initial approximation of the super-resolved spectral bands is obtained by scaling the LR-HSI using a three-dimensional interpolation filter represented by  $\boldsymbol{\Psi} \in \mathbb{R}^{s_1 s_2 s_3 N M L \times s_1 s_2 s_3 N M L}$ . This step avoids the zero padding effect by distributing information, contained in the LR-HSI, among the super-resolved spectral bands. The second step consists on reducing the spatial resolution without changing the spectral dimension. This process is represented by the matrix  $\mathbf{D}_b \in \mathbb{R}^{s_3 N M L \times s_1 s_2 s_3 N M L}$ . This is carried on to keep the dimension of the HR-HSI search space, hence reducing the computational complexity. Also, keeping the dimension avoids image noise amplification. To make the Equation (5) well posed, it is rewritten as

$$\mathbf{D}_b \boldsymbol{\Psi} \mathbf{y}_H = \mathbf{D}_b \boldsymbol{\Psi} \mathbf{D}_H \mathbf{H}_H \mathbf{x}_H + \mathbf{D}_b \boldsymbol{\Psi} \boldsymbol{\epsilon}_H \quad (8)$$

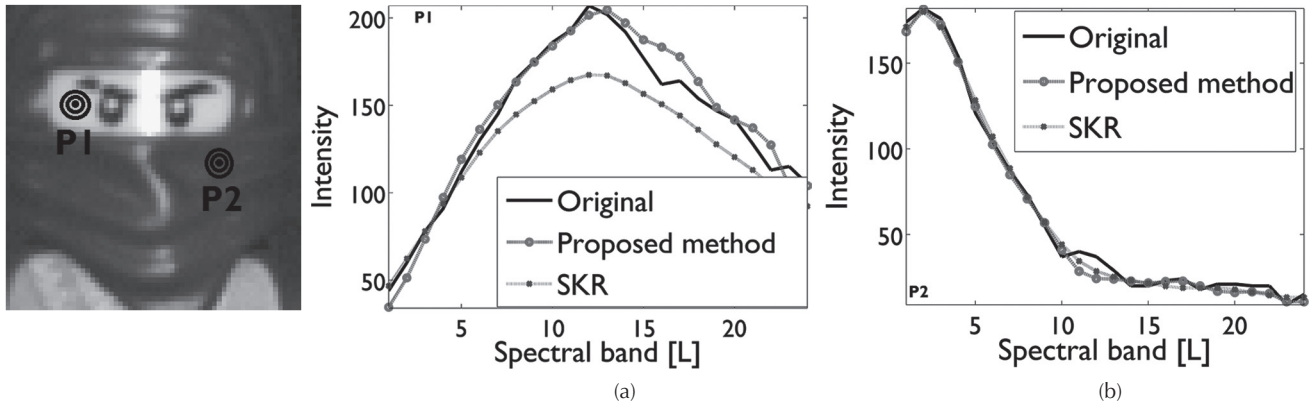


**Figure 4.** Spectral signatures at two selected spatial points (a) **P1** and (b) **P2**. These graphics shows the comparisons of SR results in the spectral dimension between SKR, and proposed method.

**Table 1.** The compact spatio-spectral super-resolution algorithm (c2sr).

Objective: Estimate HR hyperspectral image $\hat{\mathbf{x}}_H$ .
Input:
• LR hyperspectral image $\mathbf{y}_H$ .
• Interpolation factors $s_1, s_2, \text{ and } s_3$ .
Initialization:
• Set $t=0$
• Initial estimation high resolution HSI $\mathbf{x}_H^0$ , using cubic interpolation.
$\mathbf{x}_H^0 = \Psi \mathbf{y}_H$
Iteration: Perform the following $T$ times steps
• Update the HR hyperspectral image $\mathbf{x}_H^t$ , by using:
$\mathbf{x}_H^{t+1} = \mathbf{x}_H^t + \tau (\mathbf{D}_b \Psi \mathbf{D}_H \mathbf{H}_H)^T (\mathbf{D}_b \Psi \mathbf{y}_H - \mathbf{D}_b \Psi \mathbf{D}_H \mathbf{H}_H \mathbf{x}_H^t)$
• Update $t=t+1$
Result: Output of the final high-resolution HIS $\hat{\mathbf{x}}_H$ .

Therefore, the SR reconstruction consists on solving the inverse problem in the Equation (8) to estimate the HR-HSI image  $\mathbf{x}_H$ . The super-resolution reconstruction is reduced to solving the least squared problem

$$\hat{\mathbf{x}}_H = \underset{\mathbf{x}_H}{\operatorname{argmin}} \left\| \mathbf{D}_b \Psi \mathbf{y}_H - \mathbf{D}_b \Psi \mathbf{D}_H \mathbf{H}_H \mathbf{x}_H \right\|_2^2 \quad (9)$$

To obtain a solution to Equation (9), it is reformulated in a concise form using the gradient descent method, i.e.,

$$\mathbf{x}_H^{t+1} = \mathbf{x}_H^t + \tau (\mathbf{D}_b \Psi \mathbf{D}_H \mathbf{H}_H)^T (\mathbf{D}_b \Psi \mathbf{y}_H - \mathbf{D}_b \Psi \mathbf{D}_H \mathbf{H}_H \mathbf{x}_H^t) \quad (10)$$

where  $t$  represents the iteration times, and  $\tau$  stands for the step size for gradient descent. A detailed description of the C2SR algorithm is shown in Table I, the C2SR algorithm finds the images  $\hat{\mathbf{x}}_H$  in its vector representation  $\hat{\mathbf{x}}_H$ , which satisfies the constraints given in Equation (8). Further, the high-resolution image  $\hat{\mathbf{x}}_H$  can be found in function of its low-resolution version  $\hat{\mathbf{y}}_H$ . From Equation (9), we can see that there are three key procedures to obtain a local optima solution  $\hat{\mathbf{x}}_H$ : the first, is the calculation of a rescaled Low-resolution hyperspectral image of input using

a three-dimensional interpolation  $\Psi$ . The second consists on reducing the spatial resolution using  $\mathbf{D}_b$ ; and the latter is the gradient descent-based minimization to update  $\mathbf{x}_H^{t+1}$ . Computational burden could be further reduced by estimating  $(\mathbf{D}_b \Psi \mathbf{D}_H \mathbf{H}_H)^T \mathbf{D}_b \Psi \mathbf{y}_H$  at an interval rather than every time. This can significantly reduce the CPU time spent on the SR reconstruction. Moreover, computations can be more efficient if  $\Psi \mathbf{D}_H \cong 1$  is assumed. In C2SR algorithm, the initial iteration HR  $\mathbf{x}_H^0$  is estimated by using a three-dimensional interpolation  $\Psi$ , and then the vectors  $\mathbf{D}_b \Psi \mathbf{D}_H \mathbf{H}_H \mathbf{x}_H^t$  and  $\mathbf{D}_b \Psi \mathbf{y}_H$  are calculated. The update of the HR-HSI  $\mathbf{x}_H^t$  and the calculation of  $\mathbf{D}_b \Psi \mathbf{D}_H \mathbf{H}_H \mathbf{x}_H^t$  are then alternately performed until a predetermined maximum number of iterations are reached.

**Table 2.** Mean reconstruction PSNR in dB for the Legos and Ribeira images with four levels of Gaussian noise, and a super-resolution factor of  $s_1 = s_2 = s_3 = 2$ .

SNR	Image	NLM	SKR	Proposed
10	Legos	28,46	29,43	<b>30,53</b>
	Ribeira	33,29	32,94	<b>33,75</b>
15	Legos	28,81	30,02	<b>31,87</b>
	Ribeira	34,94	33,17	<b>37,59</b>
20	Legos	29,23	30,08	<b>32,22</b>
	Ribeira	35,14	36,73	<b>40,01</b>
50	Legos	29,6	30,25	<b>32,27</b>
	Ribeira	35,16	36,77	<b>41,87</b>

## Image acquisition

In this section, the performance of the proposed method is assessed in terms of the super-resolution factor, and the noise in the acquired data. For this purpose, the two traditional SR methods [NLM]-[SKR] are implemented and compared with the proposed C2SR algorithm. The SR methods were tested using the standard image databases used in (Arguello H., 2012), (Rueda-Chacón, 2014) (Rueda, 2013). The first HSI is a Lego image with  $512 \times 512$  pixels of spatial resolution and  $L=24$  spectral bands. The second

is the Ribeira city image with  $1000 \times 1000$  pixels of spatial resolution and  $L=32$  spectral bands. The Lego image was acquired using a wide-band Xenon lamp as the light source, and a visible monochromator which spans the spectral range between 450nm and 650nm. The image intensity was captured using a CCD camera AVT Marling F0033B, exhibiting  $512 \times 512$  pixels, with pixel pitch of  $9,9 \mu\text{m}$ , and 24 bits of pixel depth. The resulting test hyperspectral image  $\mathbf{x}_H$  has  $512 \times 512$  pixels of spatial resolution and  $L=24$  spectral bands. The second, the Ribeira city image was acquired using a low-noise Peltier cooled digital camera providing an  $x-y$  spatial resolution of  $1344 \times 1024$  pixels (Hamamatsu Photonics) with a fast tunable liquid-crystal filter mounted in front of the lens, together with an infrared blocking filter. The peak-transmission wavelength was varied in 10 nm steps over 400–720 nm and the bandwidth was 10 nm at 510 nm, decreasing to 7 nm at 400 nm to

16 nm at 720 nm. The resulting test hyperspectral image  $\mathbf{x}_H$  has  $1000 \times 1000$  pixels of spatial resolution and  $L=32$  spectral bands (Foster, 2004).

**Table 3.** Mean reconstruction PSNR in dB for the Legos and Ribeira images with three levels of Gaussian noise. (a) Represents the graphs of the Ribeira images reconstruction and (b) represents the graphs of the Legos images reconstruction.

SR factor	Image	NLM	SKR	Proposed
2	Legos	29,46	30,25	32,27
	Ribeira	35,16	36,77	41,87
4	Legos	24,47	28,31	29,3
	Ribeira	30,36	34,36	35,59
8	Legos	19,93	23,7	23,85
	Ribeira	25,89	28,45	29,58



**Figure 5.** Results for Lego HSI database. (a) depicts the low resolution images with sizes  $256 \times 256 \times 12$ , with a SNR factor of 50 (row 1), 15 (row 2), and 10 (row 3). The LR image are reconstructed by (b) NLM, (c) SKR, and (d) proposed method. These images are reconstructed by a super-resolution factor of  $s_1 = s_2 = s_3 = 2$ .

## Experimental results

Simulations results were analyzed in terms of Peak-Signal-to-Noise-Ratio (PSNR) in the spatial, and spectral reconstructed images (Wang, 2004). PSNR is defined as  $10\log_{10}\left(\max(x_H)^2 / MSE\right)$  wherein  $MSE$  is the mean squared error, and  $\max(x_H)$  depicts the maximum intensity of the hyperspectral image. In order to illustrate the spectral reconstruction performance, two spatial points were randomly chosen, and the spectral signatures plotted in Figure 4, these points are indicated as P1 and P2. Again, it can be seen how the curves using the proposed method are closer to the original. It is important to remark the impact of the tridimensional filters in the reconstructed spectral signature curve for hyperspectral images.

The robustness of the reconstructions with respect to the effect of noise, and decimation of the measurements is studied in the Table 2-3, and illustrated in Figure 5 and Figure 6, respectively. Gaussian noise with zero mean was added to the measurements. The Signal to Noise Ratio (SNR) is calculated according to  $SNR = 10\log_{10}\left(\frac{\mu_y - y}{\sigma_{noise}}\right)$ , where  $\mu_y$  is the mean value of the LR-HSI  $y$ , and  $\sigma_{noise}$  is the standard deviation of the signal noise. The factors of decimation used were 2,4 and 8, in the spatial and spectral dimension. The results using the proposed method indicate improvements up to 4dB in the PSNR of the reconstructed hyperspectral image compared with the results using Lanczos interpolation. The NLM and SKR methods achieve better results than Lanczos interpolation; however, these methods also have inferior performance than the proposed method. Therefore, in terms of the values of PSNR, the proposed method achieves higher performance.

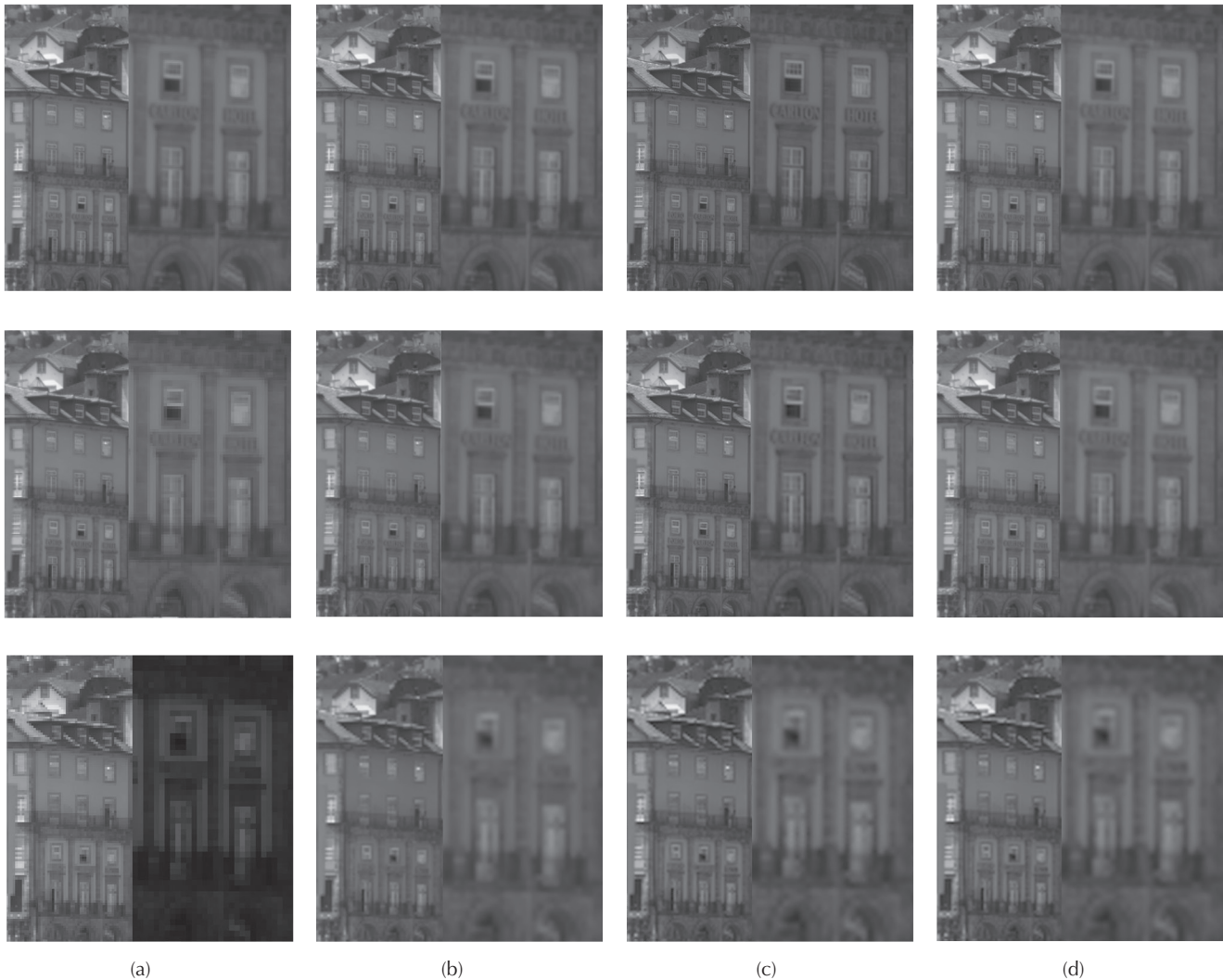


**Figure 5.** Results for Ribeira HSI database. (a) depicts the low resolution images without gaussian noise, and sizes of  $500 \times 500 \times 12$  (row 1),  $250 \times 250 \times 6$  (row 2), and  $125 \times 125 \times 3$  (row 3). The LR images are reconstructed by (b) NLM, (c) SKR, and (d) proposed method.

## Conclusions

In this paper, we present a novel SR reconstruction method for a single hyperspectral image. The proposed method incorporates the spectral reconstruction, the local spectral similarity, and the local structural regularity into a unified iterative framework for SR task. The thorough experimental results show the effectiveness of the proposed method. The proposed SR framework can be naturally extended by the following considerations: the design of three-dimensional downsampling matrix and three-dimensional interpolation matrix. The discrete mat ematical model of the LR image formation and HR reconstruction process for hyperspectral images has been proposed. This mathematical model outperforms current approaches up to 2 dB in terms of PSNR.

## Acknowledgements

The authors gratefully acknowledge the Vicerrectoría de Investigación y Extensión of the Universidad Industrial de Santander for supporting this research registered under the project title: "DISEÑO Y OPTIMIZACIÓN DE APERTURAS CODIFICADAS EN ESCALA DE GRISES PARA EL AUMENTO DEL RANGO DINÁMICO DE LAS RECONSTRUCCIONES DE IMÁGENES ESPECTRALES MUESTREADAS UTILIZANDO LA TEORÍA DE MUESTREO COMPRESIVO", (VIE 1890 code).

## References

- Akgun, T. Y. (2005). Super-resolution reconstruction of hyperspectral images. *IEEE Transactions on Image Processing*, 14(11), 1860-1875. DOI: 10.1109/TIP.2005.854479
- Arguello, H., & Arce, G. R. (2012, August). Restricted isometry property in coded aperture compressive spectral imaging. *2012 IEEE Statistical Signal Processing Workshop*, 716-719. DOI: 10.1109/SSP.2012.6319803
- Arguello, H. (2012). Spatial super-resolution in code aperture spectral imaging. *SPIE Defense, Security, and Sensing. International Society for Optics and Photonics*. 83650A-83650A. DOI: 10.1117/12.918352
- Belluco, E. (2006). Mapping salt-marsh vegetation by multispectral and hyperspectral remote sensing. *Remote sensing of environment*, 105(1), 54-67. DOI: 10.1016/j.rse.2006.06.006
- Borengasser, M., Hungate, W. S., & Watkins, R. (2007). *Hyperspectral remote sensing: principles and applications*. CRC press.
- Castrodad, A., Xing, Z., Greer, J., Bosch, E., Carin, L., & Sapiro, G. (2010 september). Discriminative sparse representations in hyperspectral imagery. *2010 IEEE International Conference on Image Processing*, 1313-1316. DOI: 10.1109/ICIP.2010.5651568
- Chakrabarti, A., & Zickler, T. (2011, June). Statistics of real-world hyperspectral images. *In Computer Vision and Pattern Recognition (CVPR)*, 48(6), 193-200. DOI: 10.1109/cvpr.2011.5995660
- Chan, J. C. W., Ma, J., Kempeneers, P., & Canters, F. (2010). Superresolution enhancement of hyperspectral CHRIS/Proba images with a thin-plate spline nonrigid transform model. *IEEE Transactions on Geoscience and Remote Sensing*, 48(6), 2569-2579. DOI: 10.1109/TGRS.2009.2039797
- Dicker, D. T., Lerner, J., Van Belle, P., Guerry, 4th, D., Herlyn, M., Elder, D. E., & El-Deiry, W. S. (2006). Differentiation of normal skin and melanoma using high resolution hyperspectral imaging. *Cancer biology & therapy*, 5(8), 1033-1038. DOI: 10.4161/cbt.5.8.3261
- Dong, W., Zhang, L., Shi, G., & Wu, X. (2011). Image deblurring and super-resolution by adaptive sparse domain selection and adaptive regularization. *IEEE Transactions on Image Processing*, 20(7), 1838-1857. DOI: 10.1109/TIP.2011.2108306
- Foster, D. H., Nascimento, S. M., & Amano, K. (2004). Information limits on neural identification of colored surfaces in natural scenes. *Visual neuroscience*, 21(03), 331-336. DOI: 10.1017/S0952523804213335
- Freeman, W. T., Jonse, T. R., & Pasztor, E. C. (2002). Example-based super-resolution. *IEEE Computer graphics and Applications*, Vol. 22(2), 56-65. DOI: 10.1109/38.988747
- Li, X. & Orchard, M. T. (2001). New edge-directed interpolation. *IEEE transactions on image processing*, Vol. 10(10), 1521-1527. DOI: 10.1109/83.951537
- Melgani, F., & Bruzzone, L. (2004). Classification of hyperspectral remote sensing images with support vector machines. *IEEE Transactions on geoscience and remote sensing*, 42(8), 1778-1790. DOI: 10.1109/TGRS.2004.831865
- Mianji, F. A. (2008). Super-resolution challenges in hyperspectral imagery. *Information Technology Journal*, 7(7), 1030-1036. DOI: 10.3923/itj.2008.1030.1036
- Protter, M. E. (2009). Generalizing the nonlocal-means to super-resolution reconstruction. *IEEE Transactions on image processing*, 18(1), 36-51. DOI: 10.1109/TIP.2008.2008067
- Rueda, H. F. (2013). On super-resolved coded aperture spectral imaging. *Society of Photo-Optical Instrumentation Engineers (SPIE) Conference Series*. DOI: 10.1117/12.2015855
- Rueda-Chacón, H. F., Vargas-García, C. A., & Arguello-Fuentes, H. (2014). Single-pixel optical sensing architecture for compressive hyperspectral imaging. *Revista Facultad de Ingeniería Universidad de Antioquia*, 73, 124-133.
- Takeda, H. F. (2007). Kernel regression for image processing and reconstruction. *IEEE Transactions on image processing*, 16(2), 349-366. DOI: 10.1109/TIP.2006.888330
- Tanaka, M. &. (2007). A fast algorithm for reconstruction-based superresolution and evaluation of its accuracy. *Systems and Computers in Japan*, 38(7), 44-52. DOI: 10.1002/scj.20662

- Turk, M., & Pentland, A. (1991). Eigenfaces for recognition. *Journal of cognitive neuroscience*, 3(1), 71-86. DOI: 10.1162/jocn.1991.3.1.71
- Underwood, E., Ustin, S., & DiPietro, D. (2003). Mapping nonnative plants using hyperspectral imagery. *Remote Sensing of Environment*, 86(2), 150-161. DOI: 10.1016/S0034-4257(03)00096-8
- Wang, Z., Bovik, A. C., Sheikh, H. R., & Simoncelli, E. P. (2004). Image quality assessment: from error visibility to structural similarity. *IEEE transactions on image processing*, 13(4), 600-612. DOI: 10.1109/TIP.2003.819861
- Winter, M. E., & Winter, E. M. (2002, August). Physics-based resolution enhancement of hyperspectral data. *In Proceedings of SPIE* (Vol. 4725, pp. 580-587).
- Zhang, K., Gao, X., Tao, D., & Li, X. (2012). Single image super-resolution with non-local means and steering kernel regression. *IEEE Transactions on Image Processing*, 21(11), 4544-4556. DOI: 10.1109/TIP.2012.2208977
- Zhao, Y. Yang, J., Zhang, Q., Song, L., Cheng, Y., & Pan, Q. (2011). Hyperspectral imagery super-resolution by sparse representation and spectral regularization. *EURASIP Journal on Advances in Signal Processing*, 1, 1. DOI: 10.1186/1687-6180-2011-87